frontiers | Frontiers in Physics

TYPE Original Research
PUBLISHED 13 October 2022
DOI 10.3389/fphy.2022.974562

OPEN ACCESS

EDITED BY
Animasaun I. L.,
Federal University of Technology, Nigeria

REVIEWED BY
Prasannakumara B. C.,
Davangere University, India
Oluwole Daniel Makinde,
Stellenbosch University, South Africa
S. Eswaramoorthi,
Dr.N.G.P. Arts and Science College, India
Khadija Maqbool,
International Islamic University, Pakistan
Anwar Shahid,
Zhejiang University of Science and Technology, China

*CORRESPONDENCE
K. Loganathan,
loganathankaruppusamy304@gmail.com

†These authors have contributed equally to this work

SPECIALTY SECTION
This article was submitted to Interdisciplinary Physics, a section of the journal Frontiers in Physics

RECEIVED 21 June 2022
ACCEPTED 21 September 2022
PUBLISHED 13 October 2022

CITATION
Loganathan K, Alessa N, Jain R, Ali F and Zaib A (2022), Dynamics of heat and mass transfer: Ree-Eyring nanofluid flow over a Riga plate with bioconvention and thermal radiation. *Front. Phys.* 10:974562. doi: 10.3389/fphy.2022.974562

Dynamics of heat and mass transfer: Ree-Eyring nanofluid flow over a Riga plate with bioconvention and thermal radiation

K. Loganathan[1*†], Nazek Alessa[2†], Reema Jain[1†], Farhan Ali[3†] and Aurang Zaib[3†]

[1]Department of Mathematics and Statistics, Manipal University Jaipur, Jaipur, India, [2]Department of Mathematical Sciences, College of Sciences, Princess Nourah Bint Abdulrahman University, Riyadh, Saudi Arabia, [3]Department of Mathematical Sciences, Federal Urdu University of Arts, Sciences & Technology, Karachi, Pakistan

Following improvements in devices used in biomedical engineering, cancer treatments, and thermal extrusion systems, this report explores the dynamics of Ree-Eyring nanofluid when subject to free convection, bioconvection, heat source, and thermal radiation over a convection-heated Riga plate. Bioconvection is assessed in light of the movement of the motile microorganisms that stabilize the dispersion of nanoparticles in the fluid. The impact of thermophoresis and Brownian motion, critical in the flow of heat and mass is also considered, together with the convective boundary condition. In many manufacturing sectors, non-Newtonian nanofluid flow is a crucial cooling component. Based on these factors, partial differential equations—the governing equations that model the transportation phenomena—are converted into nonlinear ordinary differential equations using the relevant relations. Finally, the nonlinear differential equations are solved using the homotopy analysis method (HAM), and the solutions are displayed in graphs representing distinct fluid flow parameters. It is conclusively found that the skin friction coefficient increases as the mixed convection parameter value rises, while the opposite effect is seen as the bioconvection Rayleigh number grows.

KEYWORDS

Ree-Eyring nanomaterial, Riga plate, bioconvection, thermal radiation, homotopy analysis method

Introduction

The term "nano liquid" was coined by Choi [1] and refers to the suspension of nanoparticles in standard fluid-like ethylene glycol, oil, and water. Nanomaterials have various consequences for heat transfer, such as in hybrid energy engines, microprocessors, energy engines, and in temperature diminution. Buongiorno [2] introduced two new

features to the mathematical formulation, namely Brownian motion and thermophoretic force. Then Islam et al. [3], deliberated on the MHD flow of micropolar nanofluids using a thermal mechanism between two surfaces. Alempour et al. [4] described an elliptical cross-section of spinning wall tubes to explain the behavior of a nano liquid. Entropy analysis of the Darcy-Forchheimer flow of a nanoliquid past the nonlinear sheet was conducted by Rasool et al. [5]. Numerical investigation of the slip effect of Ree-Eyring nanofluid under peristaltic flow over a curved surface was conducted by Tanvir and Malik [6]. The heat transfer enhancement accompanying nano liquid flow was scrutinized by Wang et al. [7]. Many researchers have described nano liquid flow in terms of thermal conductivity and heat transfer [8–12]. The Hall effect and impact of a chemical reaction on the physical properties of a hybrid nanofluid were discussed by Mkhatshwaet et al. [13]. Tlili et al. [14] explained the 3-D flow of Eyring-Powell nano liquid in the Darcy-Forchheimer [15] over a porous medium. The effect of Lorentz force on Ree-Eyring nanoliquid past a paraboloid surface was studied by Khan and co-workers [7]. Khan et al. [16] explored the thermal slip in the magnetized axi-symmetric flow of Oldroyd-B fluid configured by infinite stretchable disks.

Non-Newtonian flows are more efficient, due to their practical application in industrial, physiological, and technological processes. The properties of all non-Newtonian fluids are diverse, and the behaviors of all types of such fluids are depicted by a single relation. Hence different flows are given the significance of non-Newtonian liquids. Ree-Eyring fluids elucidate such behaviors with more advantages than other fluids. While the power-law model is the prominent flow model, demonstrating the shear-thinning as well as the thickening behaviors of fluids, the Ree-Eyring liquid flow is more effective in that it can be decreased to a Newtonian fluid flow [17–20]. Shao et al. [21] thus represented the thermal analysis of hydrodynamic lubrication on the Ree-Eyring fluid model, while Hayat et al. [22] scrutinized the influence of Ree-Erying flow on peristaltic transport past a rotating disk, and Ijaz et al. [23] explored the MHD flow of Ree-Eyring peristaltic propulsion. Hayat et al. [24] explained the homogenous-heterogeneous influence on the peristaltic MHD flow of Ree-Eyring fluid under chemical reactions, while the influence of a chemical reaction through Dacy-Forchheimer flow on Ree-Eyring fluid over an inclined surface was assessed by Rao et al. [25]. Some of the latest literature related to non-Newtonian models is given in References [20, 26–31].

Bioconvection is the phenomenon that occurs when up-swimming microorganisms form a smaller area denser than water. The higher portion of the surface is suspended and becomes denser due to the collection of the microorganisms. The behavior of the microorganisms in the dispersion of nanoparticles explains their remarkable applications in microsystems, biodiesel fuels, biosensors, biotechnology, and microsystems. The work of bioconvection was initiated by Wager [32] and Platt [33]. Self-thrusting microorganisms are denser than cell fluids and are inherently destabilizing, either inducing or enhancing bioconvection. The Gyrotactic microorganism has the strength of viscosity and the gravitational capacity of bottom-heavy microorganisms to move away from the vertical. The premier contribution related to bio-convention with nanoparticles under motile microorganisms is an investigation by Kuznetsov [34]. Uddin and co-workers [35] inspected the mixed convection flow of thermal slip nano liquid with microorganisms over a permeable medium. The flow of Sisko nanoparticles under microorganisms with mixed convection was then examined by Farooq et al. [36]. Exploration of the unsteady flow of nanoparticles, along with microorganisms in conjunction with nanoparticles, was carried out by Waqas et al. [37]. A study of the bioconvection flow of nanoparticles around a cone was conducted by Khan et al. [38]. The significance of Stefan flow on the bioconvection flow of nanofluids was studied by [39, 40], while the effect of viscous dissipation with the thermal radiative bioconvection flow of Casson nanofluids past a suction/injection is discussed by Kiari et al. [41]. The influence of oxytactic microorganisms in a porous medium is presented by Shaw et al [42].

The ever-increasing population expansion and the industrial revolution of the twenty-first century have led to a growing energy demand in the modern world, which is a source of concern. Traditional energy sources are to be largely replaced with clean and sustainable renewable sources, such as solar, wind, hydropower, and biogas, to meet current and future global energy needs without causing harmful environmental impacts such as pollution. Because of its affordability, its non-conventional character, and environmental friendliness, solar energy is the most pleasing renewable energy source (non-polluting). Solar energy can be transformed into heat, water, and electricity when it is acquired from nature in the form of solar radiation. Because the size of nanoparticles is less than the de Broglie wavelength, they allow deep absorption in the base fluid by scattering incident solar light. By adjusting nanoparticle size and shape to the needs of a given application, absorption efficiency can be improved. As a result, nanoparticles improve a fluid's radiative characteristics, increasing the heat transfer rate and direct absorption efficiency of solar collectors (which may be employed in commercial and household water heating applications). Furthermore, the nanofluid's solar energy absorption capability is aided by nonlinear thermal radiation. As a result, using nanofluids and including nonlinear thermal radiation increases solar energy absorption, while also increasing heat transfer rates. Furthermore, entropy reduction increases the heat transfer rate, resulting in heat transfer intensification. Combining these processes results in an increase in heat transfer rate from the sheet, and hence significantly more cooling, thereby meeting the various requirements of today's industrial world, where the quality/properties of the end products are highly dependent on the rate of cooling used in the manufacturing process (for

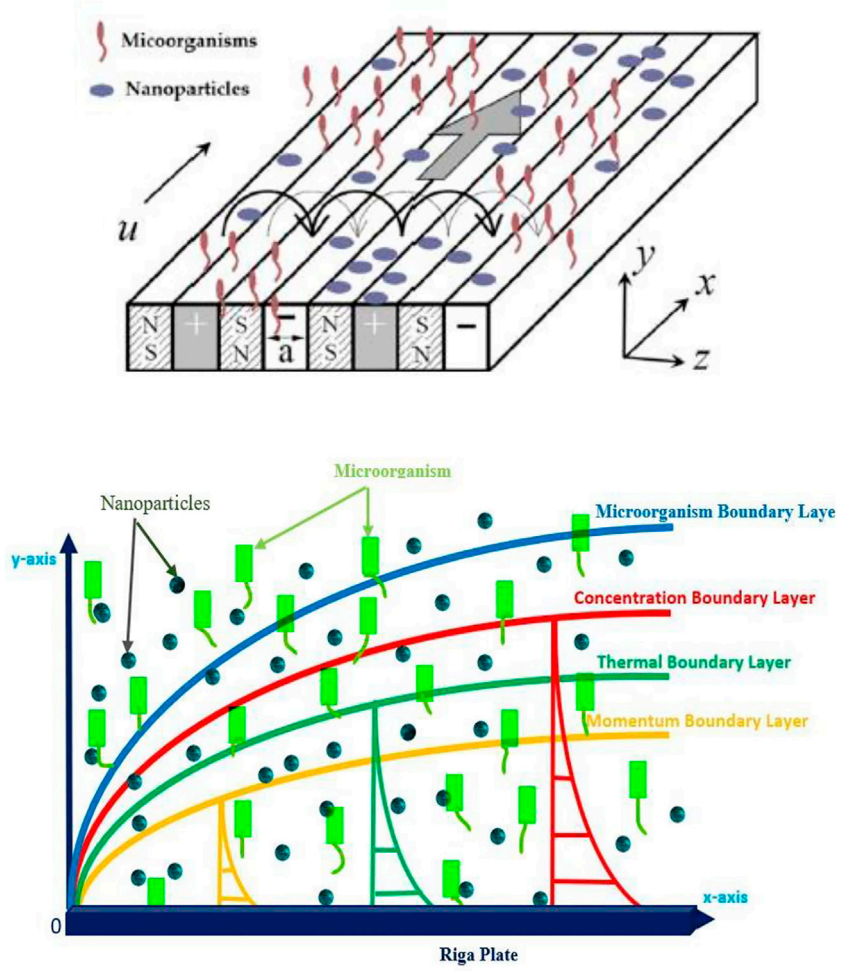

FIGURE 1
Physical sketch of the flow problem.

example, the drawing of continuous filaments through quiescent fluids, the annealing and tinning of copper wires, etc.).

While the aforementioned literature review reveals numerous articles in the area of bioconvection, bioconvection using Ree-Eyring nanofluid is rarely researched. This gap led to the present thorough analysis of the way gyrotactic microorganisms affect the flow of Ree-Eyring fluid across a Riga plate, as well as how the heat convective condition of the surface is controlled. On surfaces like stretching plates, Riga plates, and surfaces with variable thickness, nanofluids have better wetting, dispersion, and separation capabilities. The addition of the right nanoparticles to the working fluid has a significant impact on improving the thermal conductivity of the base working fluid. Such studies are important for medical, aerospace, microelectronic, and cancer thermal treatment applications. The current study concentrates on the thermal properties of Ree-Eyring nanofluid based on a mathematical model created using partial differential equations stemming from these applications. These equations are converted to ordinary differential equations by performing the proper similarity transformations, and the resulting system of equations is then solved using HAM.

Flow analysis

A steady 2-D incompressible mixed convective Ree-Eyring liquid flow along a Riga plate is considered. The flow pattern is depicted in Figure 1. The significance of the heat transportation is explored using the heat generation/absorption and convective boundary condition. The flow produced considers surface heat, wall concentration, and wall motile density as $T_f, C_W,$ and χ_w

respectively, with respective ambient temperature T_∞, ambient concentration C_∞, and ambient microorganisms χ_∞.The stress tensor for the Ree-Eyring nanofluid model is defined as

$$\tau_{ij} = \left[\mu + \frac{1}{\beta A} Sinh^{-1}\left(\frac{A}{\epsilon}\right)\right] B_R$$

where A= $\sqrt{0.5Tr\,(B_R)^2}$. The governing equations assume the following form when these assumptions and the boundary layer approximation are included in the mathematical model:

$$\frac{\partial u}{\partial x} + \frac{\partial v}{\partial y} = 0 \tag{1}$$

$$u\frac{\partial u}{\partial x} + v\frac{\partial u}{\partial y} = \frac{1}{\rho_f}\left(\mu + \frac{1}{\beta\epsilon}\right)\left(\frac{\partial^2 v}{\partial x \partial y} + 2\frac{\partial^2 u}{\partial x^2} + \frac{\partial^2 v}{\partial y^2}\right) + \frac{\pi q_0 M_0}{8\rho_f} exp\left(-\frac{\pi}{a_1} y\right) + \frac{1}{\rho_f}\Big[\times (1 - C_\infty)\rho_f \alpha g\,(T - T_\infty) - \left(\rho_p - \rho_f\right) g\,(C - C_\infty) - (\chi - \chi_\infty) g\gamma\left(\rho_m - \rho_f\right)\Big] \tag{2}$$

$$u\frac{\partial T}{\partial x} + v\frac{\partial T}{\partial y} = \frac{k}{\rho C_p}\frac{\partial^2 T}{\partial y^2} + \tau\left\{D_B\left(\frac{\partial C}{\partial y}\frac{\partial T}{\partial y}\right) + \frac{D_T}{T_\infty}\left(\frac{\partial T}{\partial y}\right)^2\right\} + \frac{Q_0}{\rho C_p}(T - T_\infty) + \frac{16\sigma * T_\infty^3}{3\rho C_p k^*}\frac{\partial^2 T}{\partial y^2} \tag{3}$$

$$u\frac{\partial C}{\partial x} + v\frac{\partial C}{\partial y} = D_B\left(\frac{\partial^2 C}{\partial y^2}\right) + \left(\frac{D_T}{T_\infty}\right)\left(\frac{\partial^2 T}{\partial y^2}\right) - \kappa_r\,(C - C_\infty) \tag{4}$$

$$u\frac{\partial \chi}{\partial x} + v\frac{\partial \chi}{\partial y} + b\frac{W_c}{(C_w - C_\infty)}\frac{\partial}{\partial y}\left(\chi\frac{\partial C}{\partial y}\right) = D_m\frac{\partial^2 \chi}{\partial y^2} \tag{5}$$

When a non-destructive layer is on a Riga plate, the dynamics of such a layer are affected, due to its movement at a specified stretching rate. Since the wall is convectively heated, the suitable boundary conditions are

$$u = u_w(x), v = 0, -k\frac{\partial T}{\partial y} = h\left(T_f - T\right), C_w = C_\infty, \chi_w = \chi_\infty \text{ at y} = 0, \quad u \to 0,\ \mathrm{T} \to T_\infty,\ C \to C_\infty,\ \chi \to \chi_\infty \text{ at y} \to \infty \tag{6}$$

If one introduces the following transformations,

$$\eta = \sqrt{\frac{a}{v}}y, u = axf'(\eta), v = -\sqrt{av}f(\eta), \theta = \frac{T - T_\infty}{T_f - T_\infty}, \phi = \frac{C - C_\infty}{C_w - C_\infty}, N = \frac{\chi - \chi_\infty}{\chi_w - \chi_\infty} \tag{7}$$

Eqs 2–5, under transformation (7), take the following form:

$$(1 + We)f''' + ff'' - f'^2 + Qe^{(-y\eta)} + \lambda\left(\theta - Nr\phi - RbN\right) = 0 \tag{8}$$

$$(1 + Rd)\theta'' + Pr\left(\phi'\theta' Nb + f\theta' + Nt\theta'^2\right) - Pr\,\varepsilon\theta = 0 \tag{9}$$

$$\phi'' + f\phi' Sc + \frac{Nt}{Nb}\phi'' - Sc\kappa\phi = 0 \tag{10}$$

$$N'' + fN' Lb - Pe\left(N'\phi' + \phi''(\Omega + N)\right) = 0 \tag{11}$$

The subject to the boundary condition is as follows:

$$f(0) = 0, f'(0) = 1, \theta'(0) = -Bi + Bi(\theta(0)), \phi(0) = 1, N(0) = 1, f'(\infty) = 0, \theta(\infty) = 0, \phi(\infty) = 0, N(\infty) = 0. \tag{12}$$

The non-dimensional variables:

$$\lambda = \frac{\alpha g(1 - C_\infty)(T_w - T_\infty)}{a^2 x}, We = \frac{1}{\mu\beta\epsilon}, Nb = \frac{\tau D_B(c_w - c_\infty)}{\nu}, Nt = \frac{\tau D_T(T_w - T_\infty)}{\nu}, Sc = \frac{\nu}{D}, Pe = \frac{bw_c}{D_m}, Rd = \frac{4\sigma^* T_\infty^1}{k_1 k^*}, Lb = \frac{\nu}{D_m}, Rb = \frac{\gamma\left(\rho_m - \rho_f\right)(N_w - N_\infty)}{\left(T_f - T_\infty\right)(1 - C_\infty)\rho_f\alpha}, Nr = \frac{\left(\rho_p - \rho_f\right)(C_w - C_\infty)}{\left(T_f - T_\infty\right)(1 - C_\infty)\rho_f\alpha}, Bi = \frac{h}{k}\sqrt{\frac{v}{a}}, Pr = \frac{\upsilon}{\alpha_f}, \Omega = \frac{\chi_\infty}{(\chi_w - \chi_\infty)}$$

C_f, Nu, Sh, and Nh are given by

$$Cf_x = \frac{2\tau_w}{\rho_f u_w^2}, Nu_x = \frac{xq_w}{k(T_w - T_\infty)}, Sh_x = \frac{xm_w}{D_B(C_w - C_\infty)}, Nh_x = \frac{xq_w}{D_m(\chi_w - \chi_\infty)} \tag{13}$$

Shear stress, heat, mass, and motile density microorganism are given by

$$\tau_w = \left(\mu + \frac{1}{\beta\epsilon}\right)\frac{\partial u}{\partial y}|_{y=0}, q_w = -k\left(\frac{\partial T}{\partial y}\right), m_w = -k\left(\frac{\partial C}{\partial y}\right), q_w = -k\left(\frac{\partial \chi}{\partial y}\right) \tag{14}$$

and are changed as follows:

$$Re_x^{0.5}Cf_x = 2(1 + We)f''(0), Re_x^{-0.5}Nu_x = -(1 + Rd)\theta'(0), Re_x^{-0.5}Sh_x = -\phi'(0), Re_x^{-0.5}Nh_x = -N'(0) \tag{15}$$

Solution methodology

Numerous numerical methods are appropriate for addressing nonlinearity difficulties. However, the most effective semi-analytical strategy for making use of these very nonlinear equations is the HAM technique. Liao [43, 44] designed the HAM technique and later changed the auxiliary parameter to have a non-zero value. The approximation rate of this solution is calculated using these variables. Additionally, the user may choose the initial premises of the solution.

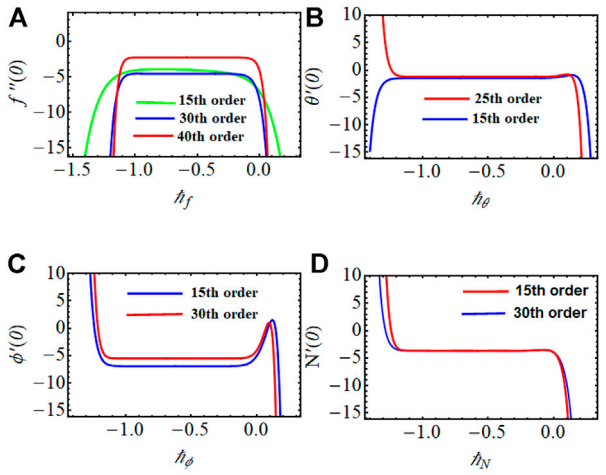

FIGURE 2
(A) $\hbar_f$ curve for $f'(\eta)$; **(B)** $\hbar_\theta$ curve for $\theta(\eta)$; **(C)** $\hbar_\phi$ curve for $\phi(\eta)$; **(D)** $\hbar_N$ curve for $N(\eta)$.

By applying this function, we can write θ, ϕ, and N in the subsequent forms:

$$f_m(\eta) = \sum_{n=0}^{\infty}\sum_{k=0}^{\infty} a_{m,n}^k \eta^k \exp(-n\eta) \tag{16}$$

$$\theta_m(\eta) = \sum_{n=0}^{\infty}\sum_{k=0}^{\infty} b_{m,n}^k \eta^k \exp(-n\eta) \tag{17}$$

$$\phi_m(\eta) = \sum_{n=0}^{\infty}\sum_{k=0}^{\infty} c_{m,n}^k \eta^k \exp(-n\eta) \tag{18}$$

$$N_m(\eta) = \sum_{n=0}^{\infty}\sum_{k=0}^{\infty} d_{m,n}^k \eta^k \exp(-n\eta) \tag{20}$$

where $a_{m,n}^k$, $b_{m,n}^k$, $c_{m,n}^k$ and $d_{m,n}^k$ are the magnitude. The linear operators, including initial guesses, are

$$\left.\begin{aligned} f_0(\eta) = 1 - e^{-\eta}, \theta_0(\eta) = \frac{Bie^{-\eta}}{1+Bi}, \phi_0(\eta) = e^{-\eta}, N_0(\eta) = e^{-\eta} \\ L(f) = f''' - f', L(\theta) = \theta'' - \theta, L(\phi) = \phi'' - \phi, L(N) = N'' - N \end{aligned}\right\} \tag{21}$$

The above auxiliary linear operators and initial guesses are

$$\left.\begin{aligned} L(f)(C_1 + C_2e^{-\eta} + C_3e^{\eta}) = 0,\ L(\theta)(C_4e^{\eta} + C_5e^{-\eta}) = 0 \\ L(\phi)(C_6e^{\eta} + C_7e^{-\eta}) = 0, L(N)(C_8e^{\eta} + C_9e^{-\eta}) = 0 \end{aligned}\right\} \tag{22}$$

where $C_i = (i = 1 - 9)$ are coefficient constants.

$$\left.\begin{aligned} \mathbf{N}_f[\bar{f}(\eta,q)] = (1+We)\frac{\partial^3\bar{f}(\eta,q)}{\partial\eta^3} + \hat{f}(\eta;q)\frac{\partial^2\bar{f}(\eta,q)}{\partial\eta^2} - \left(\frac{\partial\bar{f}(\eta,q)}{\partial\eta}\right)^2 - Qe^{-\eta} + \\ \lambda(\theta(\eta;q) - Nr\phi(\eta;q) - RbN(\eta;q)) \\ \mathbf{N}_\theta[\bar{\theta}(\eta,q)] = (1+Rd)\frac{\partial^2\bar{\theta}(\eta,q)}{\partial\eta^2} + PrNb\frac{\partial\bar{\theta}(\eta,q)}{\partial\eta}\frac{\partial\bar{\phi}(\eta,q)}{\partial\eta} + PrNt\left(\frac{\partial\bar{\theta}(\eta,q)}{\partial\eta}\right)^2 + \Pr\varepsilon\bar{\theta}(\eta,q) \\ \mathbf{N}_\phi[\bar{\phi}(\eta,q)] = \frac{\partial^2\bar{\phi}(\eta,q)}{\partial\eta^2} + Sc\,\bar{f}(\eta,q)\frac{\partial\bar{\phi}(\eta,q)}{\partial\eta} + \left(\frac{Nt}{Nb}\right)\frac{\partial^2\bar{\theta}(\eta,q)}{\partial\eta^2} - k\bar{\phi}(\eta,q) \\ \mathbf{N}_N[\bar{N}(\eta,q)] = \frac{\partial^2\bar{N}(\eta,q)}{\partial\eta^2} + Lb\,\bar{f}(\eta,q)\frac{\partial\bar{N}(\eta,q)}{\partial\eta} - Pe\left(\frac{\partial\bar{N}(\eta,q)}{\partial\eta}\frac{\partial\bar{\phi}(\eta,q)}{\partial\eta} + \frac{\partial^2\bar{\phi}(\eta,q)}{\partial\eta^2}\right)\left(\Omega + \bar{N}(\eta,q)\right) \end{aligned}\right\} \tag{23}$$

The non-zero auxiliary parameters h_f, h_θ, h_ϕ, and h_N are $q\epsilon[0,1]$

TABLE 1 Convergence table for HAM.

Order of m	$-f''(0)$	$-\theta^{(0)}$	$-\phi^{(0)}$	$-N^{(0)}$
1	0.431973	0.241666	1.219230	0.885050
5	0.433558	0.248552	1.400270	0.919057
10	0.434237	0.248180	1.400350	0.948990
15	0.434296	0.248154	1.400160	0.944370
20	0.434257	0.248152	1.400173	0.944358
25	0.434250	0.248154	1.400172	0.944355
30	0.434250	0.248154	1.400172	0.944355
35	0.434250	0.248154	1.400172	0.944355
40	0.434250	0.248154	1.400172	0.944355

$$\left.\begin{aligned} \bar{f}(\eta,0) = f_0(\eta),\ \bar{\theta}(\eta,0) = \theta_0(\eta),\ \bar{\phi}(\eta,0) = \phi_0(\eta)\ and\ \bar{N}(\eta,0) = N_0(\eta) \\ \bar{f}(\eta,1) = f(\eta),\ \bar{\theta}(\eta,1) = \theta(\eta),\ \bar{\phi}(\eta,1) = \phi(\eta), \bar{N}(\eta,1) = N(\eta) \end{aligned}\right\} \tag{24}$$

Considering the Taylor series expansion, one has

$$\left.\begin{aligned} f(\eta,q) = f_0(\eta) + \sum_{m=1}^{\infty} f_m(\eta)q^m \\ \theta(\eta,q) = \theta_0(\eta) + \sum_{m=1}^{\infty} \theta_m(\eta)q^m \\ \phi(\eta,q) = \phi_0(\eta) + \sum_{m=1}^{\infty} \phi_m(\eta)q^m \\ N(\eta,q) = N_0(\eta) + \sum_{m=1}^{\infty} N_m(\eta)q^m \end{aligned}\right\} \tag{25}$$

$$\left.\begin{aligned} f_m(\eta) = \frac{1}{m!}\frac{\partial^m f(\eta;q)}{\partial\eta^m}\bigg|_{q=0},\ \theta_m(\eta) = \frac{1}{m!}\frac{\partial^m\theta(\eta;q)}{\partial\eta^m}\bigg|_{q=0}, \phi_m(\eta) \\ = \frac{1}{m!}\frac{\partial^m\phi(\eta;q)}{\partial\eta^m}\bigg|_{q=0}, \phi_m(\eta) = \frac{1}{m!}\frac{\partial^m N(\eta;q)}{\partial\eta^m}\bigg|_{q=0} \end{aligned}\right\} \tag{26}$$

We ensure that h_f, h_θ, h_ϕ,and h_N are chosen correctly, such that Eq. 25 converges at $q = 1$. Then we have

$$\left.\begin{aligned} f(\eta) = f_0(\eta) + \sum_{m=1}^{\infty} f_m(\eta), \theta(\eta) = \theta_0(\eta) + \sum_{m=1}^{\infty} \theta_m(\eta) \\ \phi(\eta) = \phi_0(\eta) + \sum_{m=1}^{\infty} \phi_m(\eta), N(\eta) = N_0(\eta) + \sum_{m=1}^{\infty} N_m(\eta) \end{aligned}\right\} \tag{27}$$

The general solutions can be explained as

$$\left.\begin{aligned} f_m(\eta) - f_m^*(\eta) = C_1 + C_2\exp(\eta) + C_3\exp(-\eta) \\ \theta_m(\eta) - \theta_m^*(\eta) = C_4\exp(\eta) + C_5\exp(-\eta) \\ \phi_m(\eta) - \phi_m^*(\eta) = C_6\exp(\eta) + C_7\exp(-\eta) \\ N_m(\eta) - N_m^*(\eta) = C_8\exp(\eta) + C_9\exp(-\eta) \end{aligned}\right\} \tag{28}$$

where f_m^*, θ_m^*, ϕ_m^*, and N_m^* are the special solutions.

Convergence of homotopy solution

The study of auxiliary variables h_f, h_θ, h_ϕ, and h_N depends on adjusting and controlling convergence. The acceptable range of convergence values are used to draw the h-graphs. Figures 2A–D show that the appropriate values of h_f, h_θ, h_ϕ, and h_N are $-1.5 < h_f < 0.1, -1.5 < h_\theta < 0.1, -1.3 < h_\phi < 0.1, -1.2 < h_N < 0.1$. Table 1

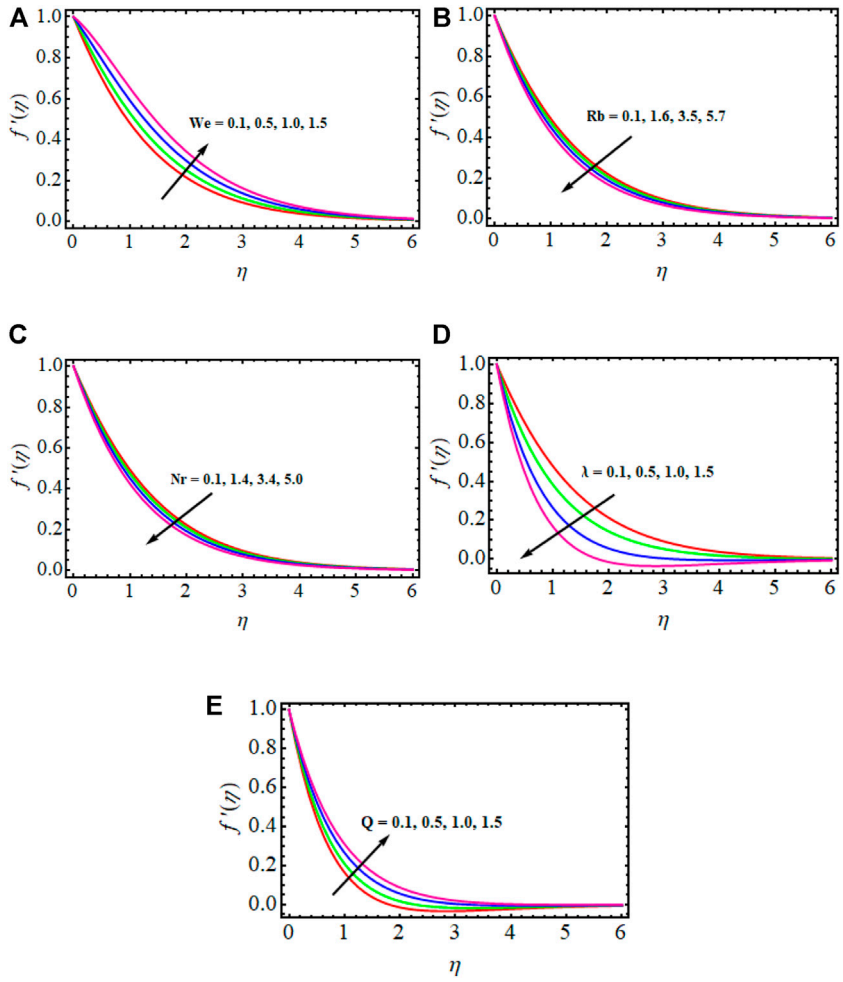

FIGURE 3
Alteration of *We*, *Rb*, *Nr*, λ, and *Q* with velocity profile $f'(\eta)$.

evaluates the convergence of the series solution when $h_f = -0.65$, $h_\theta = h_\phi = -0.55$, $h_N = -0.7$

Result and discussion

The significance of numerous physical variables is elucidated in Figures 3–11. These physical parameters are sketched for velocity, temperature, concentration, and microorganism profiles for several magnitudes of variables. Table 2 compares present findings with past outcomes under certain conditions. We noted a good agreement.

Figures 3A–E show the impact of the parameters *We*, *Rb*, *Nr*, λ,and *Q* on the velocity field $f'(\eta)$. Enhancement in We results $f'(\eta)$ and momentum layer thickness is also enhanced. Physically, a greater velocity minimizes the viscous force, due to this velocity shows increment. Figure 3B shows there is no development when exceeding the value of the bioconvection Rayleigh number. Figure 3C exhibits the impact of the buoyancy ratio parameter *Nr*, leading to reduction in the velocity profile. The varied effect of the mixed convection λ variable on the velocity profile is shown in Figure 3D. From the figure, it is clear that the augmented magnitude of λ depreciates the velocity profile. Physically, an uplift in λ obtains a higher thermal bounce force, due to the increment in the velocity of the fluid. The impact of the modified Hartman number *Q* on velocity distribution is illustrated in Figure 3E. Velocity distribution displays behavior of increased magnitude. With additional momentum, boundary layer thickness is also enhanced.

The performance of the thermal layer $\theta(\eta)$ against the values of the variables *We*, *Nb*, *Nt*, *Rd*, *Bi*, and *Pr* is shown in Figures 4A–F. From Figure 4B, it can be observed that temperature

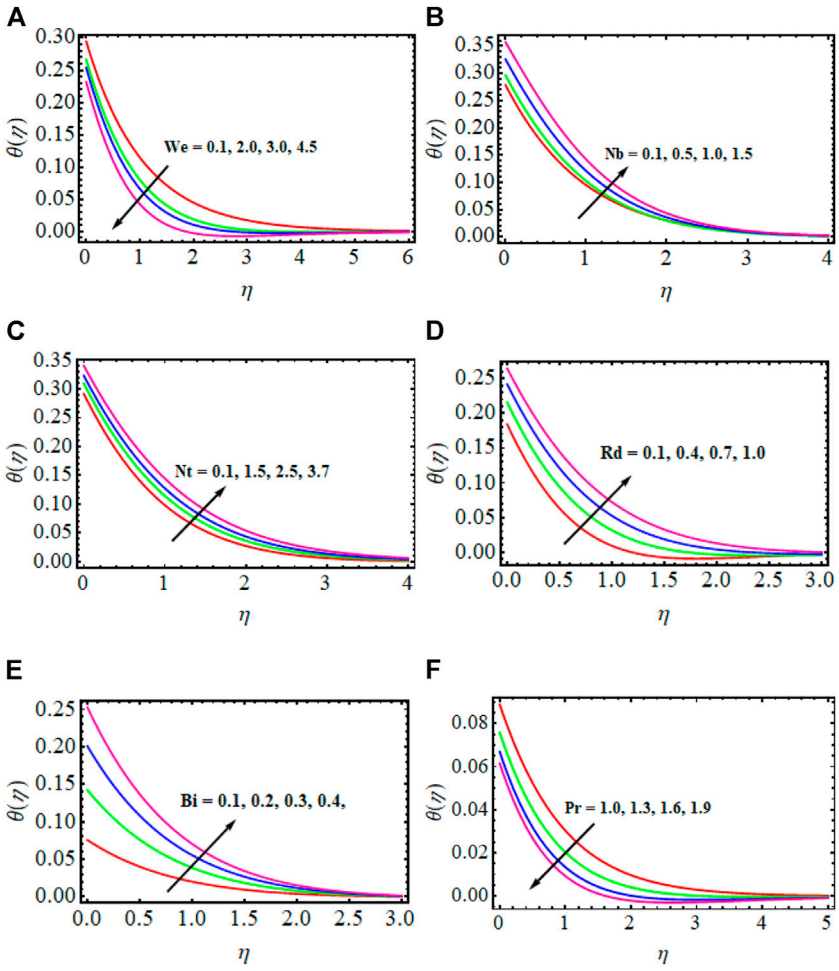

FIGURE 4
Alteration of *We*, *Nb*, *Nt*, *Rd*, *Bi*, and *Pr* with temperature profile (η).

profiles increase the function of *We*. The temperature profile improves when the Brownian motion *Nb* is increased, as shown in Figure 4B. The value of *Nb* grows as the thermal layer and boundary layer thickness increases. As the value of *Nb* rises, the intensity of this hectic movement increases, increasing the kinetic energy of the nanoparticles and therefore improving the temperature field. Figure 4C reveals that when the thermophoresis parameter increases, the concentration field and solutal boundary layer thickness accelerate. For greater levels, both the temperature and the thickness of the thermal boundary layer display distinct behaviors. Thermophoresis is a process by which heated particles are drawn away from a hot surface into a cool area. C thermal radiation is shown in Figure 4D. The raising values of *Rd* uplifts the thermal layer. The escalated value of *Rd* obtains inside heat that is the reason for the acceleration. The estimation of the *Bi* effect on $\theta(\eta)$ is revealed in Figure 4E. An increment in the value of *Bi* causes enhancement of the thermal layer and boundary layer thickness. The Biot is described as the proportion of conductive resistance inside the surface over the conductive resistance outside the surface. The impact of the Prandtl number *Pr* on the temperature profile is shown in Figure 4F. The temperature profile and the thickness of the thermal boundary layer are both reduced as the Prandtl number is increased. Thermal diffusivity reduces when the Prandtl number rises, resulting in a drop in temperature profile.

A view of the impact of $\phi(\eta)$ against the fluctuation of *We*, *Nb*, *Nt*, *k*, and *Sc* is given in Figures 5A–E. The concentration profile decays with larger *We* values, as shown in Figure 5A. For modest levels of the Brownian motion parameter, the leading behavior of the concentration profile is shown in Figure 5B. The collision of the fluid particles increases, and the concentration profile falls when the Brownian motion parameter *Nb* is increased. Figure 5C illustrates the effect of the

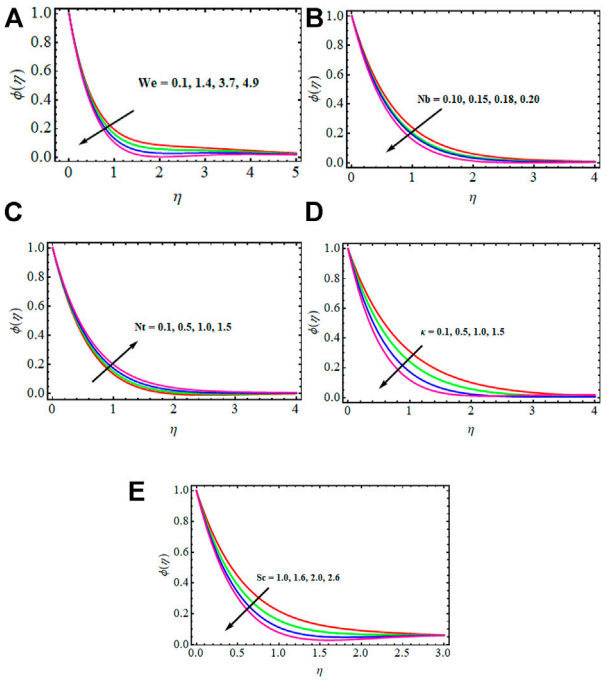

FIGURE 5
Alteration of *We*, *Nb*, *Nt*, κ, and *Sc* with concentration profile (η).

thermophoresis parameter *Nt* on the concentration field. It is discovered that when the thermophoresis parameter increases, the concentration field and solutal boundary layer thickness accelerate. For larger levels, both the temperature and the thickness of the thermal boundary layer have distinct behaviors. Thermophoresis is a process by which heated particles are drawn away from a hot surface and into a cool area. The impact of κ and *Sc* on $\phi(\eta)$ has been plotted in Figures 5D,E. Increasing value of κ and *Sc* reduces the concentration profile (η). A large value for the parameter κ reduces the mass transfer rate due to this concentration profile reduction. It is clear from the figure that the magnitude of *Sc* affects the proportion of thermal diffusivity *vis-a-vis* mass diffusivity.

Figures 6A–D are plotted to display *We*, *Lb*, Ω, and *Pe* against the microorganism density profiles. The larger *We* microorganism density profile reductions can be seen in Figure 6A. From Figure 6B, we notice the impact of *Pe* on microorganism density profile (η). The Peclet number has dominant influence when examining the swimming strength of microorganisms in the diffusion of microorganisms. Diffusion is the phenomenon that accelerates movement from a larger concentration to a lower concentration. It is noticed that diffusion of microorganism density reduces in face of the mounting value of *Pe*. Increased depreciation in the motile density $N(\eta)$ can be seen in Figure 6B. Figure 6C elucidates the consequences of the Bioconvection Schmidt number *Lb* on

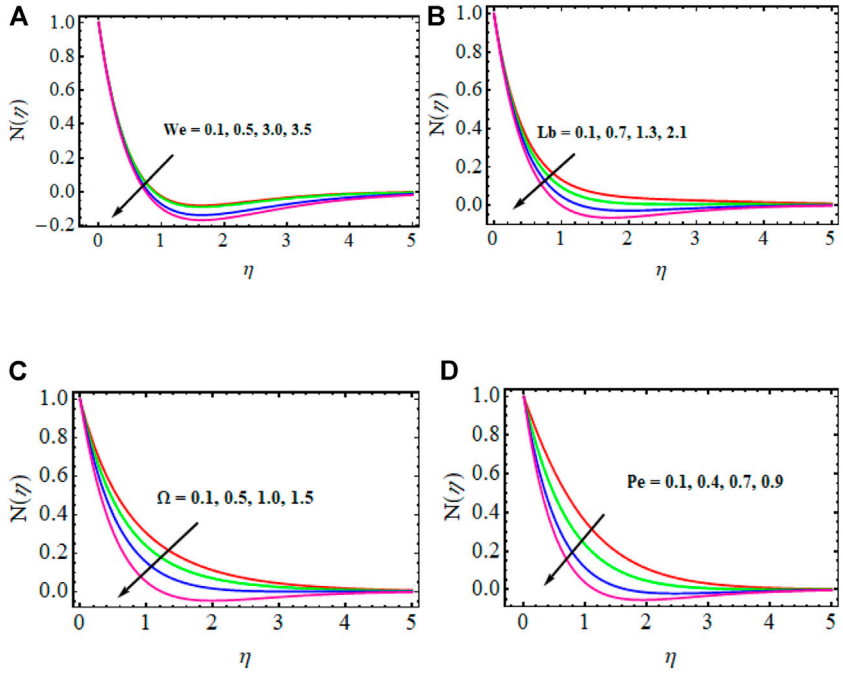

FIGURE 6
Alteration of *We*, *Lb*, Ω, and *Pe* with $N(\eta)$.

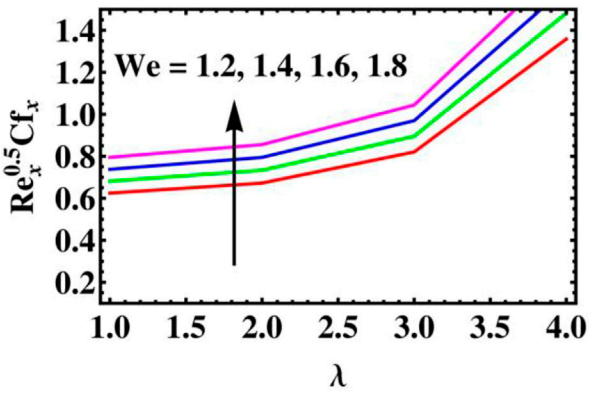

FIGURE 7
Alteration of γ with skin friction.

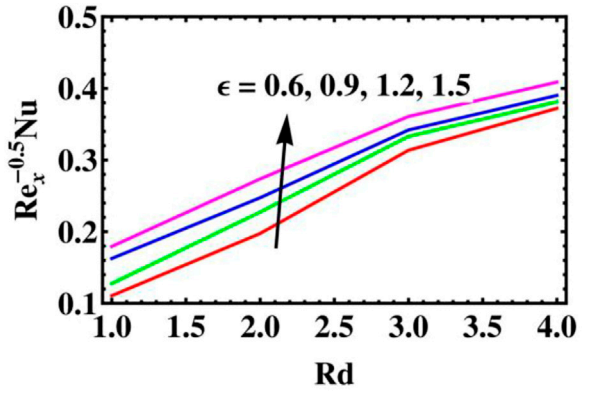

FIGURE 8
Alteration of ε with Nusselt number.

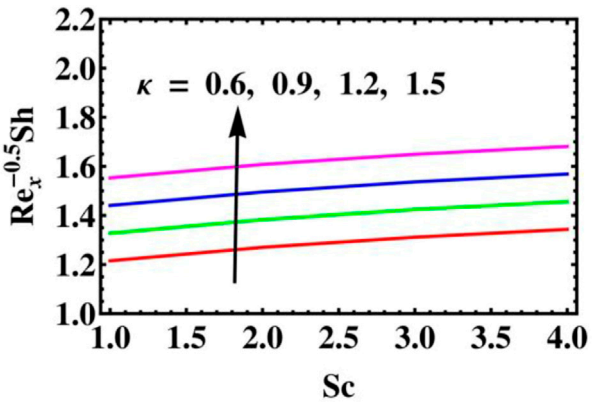

FIGURE 9
Alteration of κ with Sherwood number.

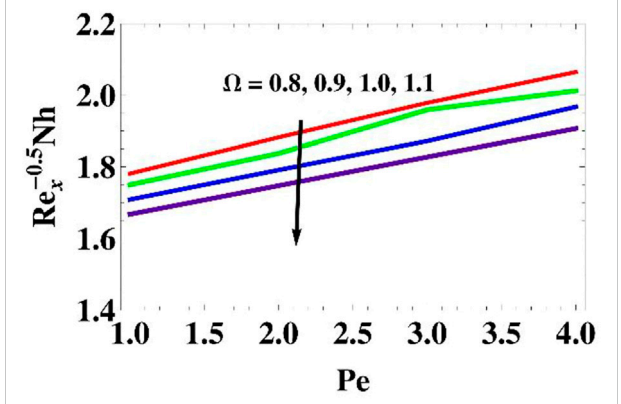

FIGURE 10
Alteration of Ω with motile microorganisms.

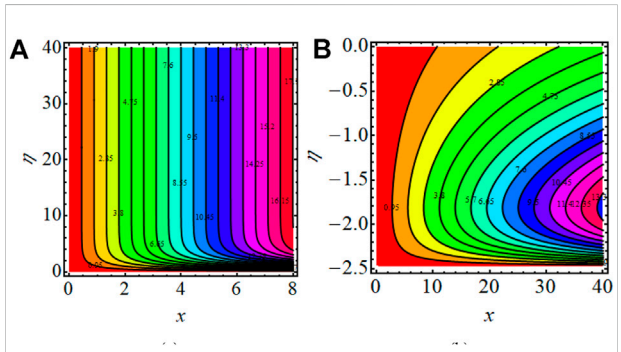

FIGURE 11
(A,B) We = 0.5 and Rd = 0.7 for stream line and isotherm line.

TABLE 2 Comparison of current findings with earlier results for $-\theta'(0)$ under special cases.

Pr $-\theta'(0)$

	Yusuf et al. [45]	Abel et al. [46]	Present results
1	1.00000000	1.000174	1.000000
2	1.52282796	1.523090	1.522759
3	1.92377603	1.923609	1.923612

the motile microorganisms (η). From Figure 6D, it can be seen that an augmentation in Lb causes a depreciation in the diffusivity of microorganisms due to this reduction in the motile microorganism profile.

Figures 7–10 exhibit variations of We and λ on f_x. From Figure 7it is noted that larger values of We and λ are maximized in f_x . Figure 8 studies the influence of Nu_x on ε against Rd. The larger values of Rd and ε reduce the Nusselt number. Figure 9 gives the impact of κ and Sc on Sh_x. It is

observed that the rate of mass transport is enhanced by increasing the value of κ and Sc. The impact of Pe and Ω on Nh_x can be viewed in Figure 10, where it is seen that the Nh_x surges for the given value of Pe and Ω.

The streamlines are tangent curves to the local instantaneous velocity field. The formation of an inner mixing bolus within a fluid surrounded by streamlines is referred to as trapping. Finally, Figures 11A,B present the streamlines and isotherm pattern. It is noted that the lines increase when $We = 1.5$. The streamlined patterns are simple curves and close to the surface. Figure 11B shows that isotherm line for a value of = 0.5.

Conclusion

This study explored the dynamics of Ree-Eyring nanofluid subject to free convection, bioconvection, heat source, and thermal radiation over a convectively heated Riga plate, with emphasis on the attributes of heat and mass transfer. The interesting significance of thermal radiative and chemical reactions are also studied in terms of temperature and concentration profiles. The homotopy analysis method (HAM) is used to obtain the series solution of the transport phenomenon.

- ➢ Fluid velocity accelerates when elevating the values of the Weissenberg number, and it deteriorates when strengthening the mixed convection parameter.
- ➢ Fluid temperature surges upward when enhancing the radiation parameter and Biot number, while the opposite impact is found for higher Brownian moment and the thermophoretic parameters.
- ➢ Brownian moment and the thermophoretic parameters lead to decrepitude in the nanoparticle concentration
- ➢ The motile microorganisms fall downwards when the Weissenberg number and Peclet number rise.
- ➢ The skin friction coefficient improves when enhancing the values of mixed convection parameters, and the opposite occurs when increasing the bioconvection Rayleigh number.

Data availability statement

The raw data supporting the conclusion of this article will be made available by the authors, without undue reservation.

Author contributions

All authors listed have made a substantial, direct, and intellectual contribution to the work and approved it for publication.

Funding

Princess Nourah Bint Abdulrahman University Researchers Supporting Project number (PNURSP2022R59), Princess Nourah Bint Abdulrahman University, Riyadh, Saudi Arabia.

Conflict of interest

The authors declare that the research was conducted in the absence of any commercial or financial relationships that could be construed as a potential conflict of interest.

Publisher's note

All claims expressed in this article are solely those of the authors and do not necessarily represent those of their affiliated organizations, or those of the publisher, the editors, and the reviewers. Any product that may be evaluated in this article, or claim that may be made by its manufacturer, is not guaranteed or endorsed by the publisher.

References

1. Choi SUS, Eastman JA, Enhancing thermal conductivity of fluids with nanoparticles. In: 1995 International mechanical engineering congress and exhibition; San Francisco, CA, 12-17 November 1995; ASME Publications-Fed (1995). p. 99–106.

2. Buongiorn J. Convective transport in nanofluids. *J Heat Transfer* (2006) 28: 240–50. doi:10.1115/1.2150834

3. Islam S, Khan A, Deebani W, Bonyah E, Alreshidi NA, Shah Z. Influences of Hall current and radiation on MHD micropolar non-Newtonian hybrid nanofluid flow between two surfaces. *AIP Adv* (2020) 10(5):055015. doi:10.1063/1.5145298)

4. Alempour SM, Arani AAA, Najafizadeh MM. Numerical investigation of nanofluid flow characteristics and heat transfer inside a twisted tube with elliptic cross section. *J Therm Anal Calorim* (2020) 140:1237–57. doi:10.1007/s10973-020-09337-z

5. Rasool G, Shafiq A, Khan I, Baleanu D, Nisar KS, Shahzadi G. Entropy generation and consequences of MHD in Darcy-Forchheimer nanofluid flow bounded by non-linearly stretching surface. *Symmetry* (2020) 12(4):652. doi:10.3390/sym12040652

6. Tanveer A, Malik MY. Slip and porosity effects on peristalsis of MHD Ree-Eyring nanofluid in curved geometry. *Ain Shams Eng J* (2021) 12(1):955–68. doi:10.1016/j.asej.2020.04.008

7. IjazKhan M, Kadry S, Chu YM, Khan WA, Kumar A. Exploration of Lorentz force on a paraboloid stretched surface in flow of Ree-Eyring nanomaterial. *J Mater Res Technol* (2020) 9(5):10265–75. doi:10.1016/j.jmrt.2020.07.017

8. Nadeem S, Khan MN, Abbas N. Transportation of slip effects on nanomaterial micropolar fluid flow over exponentially stretching. *Alexandria Eng J* (2020) 59: 3443–50. doi:10.1016/j.aej.2020.05.024

9. Waqas H, Imran M, Khan SU, Shehzad SA, Meraj MA. Slip flow of maxwell viscoelasticity-based micropolar nanoparticles with porous medium: A numerical study. *Appl Math Mech* (2019) 40(9):1255–68. doi:10.1007/s10483-019-2518-9

10. Nadeem S, Abbas N, Malik MY. Heat transport in CNTs based nanomaterial flow of non-Newtonian fluid having electro magnetize plate. *Alexandria Eng J* (2020) 59:3431–42. doi:10.1016/j.aej.2020.05.022

11. Hayat T, Yaqoob R, Qayyum S, Alsaedi A. Entropy generation optimization in nanofluid flow by variable thicked sheet. *Physica A: Stat Mech its Appl* (2020) 551: 124022. doi:10.1016/j.physa.2019.124022

12. Alic F. Entransy dissipation analysis and new irreversibility dimension ratio of nanofluid flow through adaptive heating elements. *Energies* (2020) 13(1):114. doi:10.3390/en13010114

13. Mkhatshwa MP, Motsa SS, Ayano MS, Sibanda P. MHD mixed convective nanofluid flow about a vertical slender cylinder using overlapping multi-domain spectral collocation approach. *Case Stud Therm Eng* (2020) 18:100598. doi:10.1016/j.csite.2020.100598)

14. Tlili I, Shahmir N, Ramzan M, Kadry S, Kim JY, Nam Y, et al. A novel model to analyze Darcy Forchheimer nanofluid flow in a permeable medium with Entropy generation analysis. *J Taibah Univ Sci* (2020) 14(1):916–30. doi:10.1080/16583655.2020.1790171

15. Amjad M, Zehra I, Nadeem S, Abbas N. Thermal analysis of Casson micropolar nanofluid flow over a permeable curved stretching surface under the stagnation region. *J Therm Anal Calorim* (2020) 143:2485–97. doi:10.1007/s10973-020-10127-w

16. Khan I, Ullah KS, Chu YM, Nisar KS, Al-Khaled K. Oldroyd-B nanofluid-flow between stretching disks with thermal slip and multiple flow features. *Therm Sci* (2020) 24(1):83–94. doi:10.2298/tsci20s1083k

17. Bhatti MM, Ali Abbas M, Rashidi MM. Combine effects of Magnetohydrodynamics (MHD) and partial slip on peristaltic Blood flow of Ree-Eyring fluid with wall properties. *Eng Sci Tech Int J* (2016) 19:1497–502. doi:10.1016/j.jestch.2016.05.004

18. Yoon HK, Ghajar AJ. A note on the Powell-Eyring fluid model. *Int Commun Heat Mass Transfer* (1987) 14:381–90. doi:10.1016/0735-1933(87)90059-5

19. Akbar NS, Nadeem S. Characteristics of heating scheme and mass transfer on the peristaltic flow for an Eyring -Powell fluid in an endoscope. *Int J Heat Mass Transf* (2012) 55:375–83. doi:10.1016/j.ijheatmasstransfer.2011.09.029

20. Loganathan K, Mohana K, Mohanraj M, Sakthivel P, Rajan S. Impact of third-grade nanofluid flow across a convective surface in the presence of inclined Lorentz force: An approach to entropy optimization. *J Therm Anal Calorim* (2020) 144(5): 1935–47. doi:10.1007/s10973-020-09751-3

21. Wang S, Cusano CC, Conry TF. Thermal analysis of elastohydrodynamic lubrication of line contacts using the Ree-Eyring fluid model. *J Tribol* (1991) 113: 232–42. doi:10.1115/1.2920611

22. Hayat T, Zahir H, Alsaedi A, Ahmad B. Heat transfer analysis on peristaltictransport of Ree-Eyring fluid in rotating frame. *Chin J Phys* (2018) 55: 1894–907. doi:10.1016/j.cjph.2017.08.016

23. Ijaz N, Zeeshan A, Bhatti MM. Peristaltic propulsion of particulate non Newtonian Ree-Eyring fluid in a duct through constant magnetic field. *Alexandria Eng J* (2017) 57(2):1055–60. doi:10.1016/j.aej.2017.02.009

24. Hayat T, Akram J, Alsaedi A, Zahir H. Endoscopy and homogeneous heterogeneous reactions in MHD radiative peristaltic activity of Ree-Eyring fluid. *Results Phys* (2018) 8:481–8. doi:10.1016/j.rinp.2017.12.056

25. Purna Chandar Rao D, Thiagarajan S, Srinivasa Kumar V. Darcy–Forchheimer flow of ree–eyring fluid over an inclined plate with chemical reaction: A statistical approach. *Heat Transf* (2021) 50:7120–38. doi:10.1002/htj.22220

26. Shawky HM. Pulsatile flow with heat transfer of dusty magnetohydrodynamic Ree Eyring fluid through a channel. *Heat Mass Transfer* (2009) 45:1261–9. doi:10.1007/s00231-009-0502-0

27. Hsiao KL. To promote radiation electrical MHD activation energy thermal extrusion manufacturing system efficiency by using Carreau-Nanofluid with parameters control method. *Energy* (2017) 130:486–99. doi:10.1016/j.energy.2017.05.004

28. Loganathan K, Rajan S. An entropy approach of Williamson nanofluid flow with Joule heating and zero nanoparticle mass flux. *J Therm Anal Calorim* (2020) 141:2599–612. doi:10.1007/s10973-020-09414-3

29. B-Chakra E, C-Barrioz J, Mazuyer D, Jarnias F, Bouffet A. A non-Newtonian model based on Ree–Eyring theory and surface effect to predict friction in elastohydrodynamic lubrication. *Tribol Int* (2010) 43:1674–82. doi:10.1016/j.triboint.2010.03.016

30. Loganathan K, Sivasankaran S, Bhuvaneshwari M, Rajan S. Second-order slip, cross-diffusion and chemical reaction effects on magneto-convection of Oldroyd-B liquid using Cattaneo–Christov heat flux with convective heating. *J Therm Anal Calorim* (2019) 136:401–9. doi:10.1007/s10973-018-7912-5

31. Hsiao KL. Combined electrical MHD heat transfer thermal extrusion system using Maxwell fluid with radiative and viscous dissipation effects. *Appl Therm Eng* (2017) 112:1281–8. doi:10.1016/j.applthermaleng.2016.08.208

32. Wager H. On the effect of gravity upon the movements and aggregation of euglena viridis, ehrb., and other micro-organisms. *Philos Trans R Soc B* (1911) 201: 333–90. doi:10.1098/rstb.1911.0007

33. Platt JR. Bioconvection patterns in cultures of free-swimming organisms. *Science (New York, N.Y.)* (1961) 133:1766–7. doi:10.1126/science.133.3466.1766

34. Kuznetsov AV. The onset of nanofluid bioconvection in a suspension containing both nanoparticles and gyrotactic microorganisms. *Int Commun Heat Mass Transfer* (2010) 37(10):1421–5. doi:10.1016/j.icheatmasstransfer.2010.08.015

35. Uddin MJ, Alginahi Y, Bég O, Kabir MN. Numerical solutions for gyrotactic bioconvection in nanofluid-saturated porous media with Stefan blowing and multiple slip effects. *Comput Math Appl* (2016) 72(10):2562–81. doi:10.1016/j.camwa.2016.09.018

36. Farooq S, Hayat T, Alsaedi A, Ahmad B. Numerically framing the features of second order velocity slip in mixed convective flow of Sisko nanomaterial considering gyrotactic microorganisms. *Int J Heat Mass Transf* (2017) 112: 521–32. doi:10.1016/j.ijheatmasstransfer.2017.05.005

37. Waqas H, Khan SU, Imran M, Bhatti MM. Thermally developed Falkner–Skan bioconvection flow of a magnetized nanofluid in the presence of a motile gyrotactic microorganism: Buongiorno's nanofluid model. *Phys Scr* (2019) 94(11):115304. doi:10.1088/1402-4896/ab2ddc

38. Khan WA, Rashad AM, Abdou MMM, Tlili I. Natural bioconvection flow of a nanofluid containing gyrotactic microorganisms about a truncated cone. *Eur J Mech - B/Fluids* (2019) 75:133–42. doi:10.1016/j.euromechflu.2019.01.002

39. Amirsom NA, Uddin MJ, Ismail AI. MHD boundary layer bionanoconvective non-Newtonian flow past a needle with Stefan blowing. *Heat Transfer-asian Res* (2019) 48(2):727–43. doi:10.1002/htj.21403

40. Dero S, Uddin MJ, Rohni AM. Stefan blowing and slip effects on unsteady nanofluid transport past a shrinking sheet: Multiple solutions. *Heat Trans Asian Res* (2019) 48(4):2047–66. doi:10.1002/htj.21470

41. Kairi RR, Shaw S, Roy S, Raut S. Thermo-solutalmarangoni impact on bioconvection in suspension of gyrotactic microorganisms over an inclined stretching sheet. *J Heat Transfer* (2020) 143(3). doi:10.1115/1.4048946

42. Shaw S, Kameswaran PK, Narayana M, Sibanda P. Bioconvection in a non-Darcy porous medium saturated with a nanofluid and oxytactic micro-organisms. *Int J Biomath* (2014) 7(01):1450005. doi:10.1142/s1793524514500053

43. Liao S. *Homotopy analysis method in nonlinear differential equations*. Germany: Higher Education Press: Berlin/Heidelberg (2012). p. 153–65.

44. Zhao Y, Liao S. On the HAM-based mathematica package BVPh for coupled nonlinear ODEs. In: AIP Conference Proceedings; College Park, MD, USA, 26 September 2012; American Institute of Physics (2012). p. 1842–4. doi:10.1063/1.4756540

45. Yusuf TA, Gbadeyan JA. Entropy generation on maxwell fluid flow past an inclined stretching plate with slip and convective surface conditon: Darcy-forchheimer model. *Nano Hybrids and Composites* (2019) 26:62–83. doi:10.4028/www.scientific.net/nhc.26.62

46. Abel MS, Tawade JV, Nandeppanavar MM. MHD flow and heat transfer for the upper-convected Maxwell fluid over a stretching sheet. *Meccanica* (2012) 47(2): 385–93. doi:10.1007/s11012-011-9448-7

Nomenclature

We Weissenberg number, Dimensionless
λ Mixed convection parameter, Dimensionless
Nb Brownian motion parameter, Dimensionless
Nt Thermophoresis parameter, Dimensionless
Nr Buoncy ratio parameter, Dimensionless
Pr Prandtl number, Dimensionless
Rd Radiation parameter, Dimensionless
Rb Bioconvection Rayleigh number, Dimensionless
Sc Schmidt number, Dimensionless
Lb Bioconvection Schmidt number, Dimensionless
Pe Bioconvection Peclet number, Dimensionless
κ Chemical reaction parameter, Dimensionless
ε Heat source/sink parameter, Dimensionless
Cf_x Skin friction coefficient, Dimensionless
Nu_x Nusselt number, Dimensionless
Sh_x Sherwood number, Dimensionless
Nh_x Microorganism density number, Dimensionless
f Dimensionless velocity profile, Dimensionless
θ Dimensionless temperature profile, Dimensionless
ϕ Dimensionless concentration profile, Dimensionless
N Dimensionless microorganism profile, Dimensionless
Ω Microorganism concentration difference parameter, Dimensionless
η Similarity variable, Dimensionless
u, v Components of velocity along x, y direction $m\,s^{-1}$
τ Ratio of the effective heat capacity, Dimensionless
v Kinematic viscosity, $m^2\,s^{-1}$
a Stretching rate, s^{-1}
ρ Density, kgm^{-1}
ρ_f Density of nanofluid, kgm^{-3}
ρ_p Density of nanoparticles, kgm^{-3}
ρ_m Density of microorganism's particles, kgm^{-3}
C_p Specific heat, $J\,kg^{-1}\,K^{-1}$
D_B Brownian diffusion coefficient, $m^2\,s^{-1}$
D_T Thermophoretic diffusion coefficient, $m^2\,s^{-1}$
D_m Microorganism's diffusion coefficient, $m^2\,s^{-1}$
C Concentration, kgm^{-3}
C_∞ Ambient concentration, kgm^{-3}
C_w Surface concentration of nanoparticles, kgm^{-3}
k Thermal conductivity, $m\,kgs^{-3}K^{-1}$
T Temperature, K
T_∞ Ambient temperature, K
T_f Surface heat, K
$h(t)$ Coefficient of heat transfer W, $m^{-2}K^{-1}$
χ Microorganism's profile, Dimensionless
χ_w Surface concentration of microorganisms, kgm^{-3}
χ_∞ Ambient concentration of microorganisms, kgm^{-3}
W_c Maximum cell swimming speed, $m\,s^{-1}$
x, y Cartesian coordinates, m
u_w Velocity of the sheet, $m\,s^{-1}$